
Article:
Cercola, Rosaria, Matthews, Edward and Dessent, Caroline E H orcid.org/0000-0003-4944-0413 (2017) Photoexcitation of Adenosine 5'-Triphosphate Anions in Vacuo : Probing the Influence of Charge State on the UV Photophysics of Adenine. Journal of Physical Chemistry B. pp. 5553-5561. ISSN 1520-6106

https://doi.org/10.1021/acs.jpcb.7b03435

Photoexcitation of Adenosine-5'-Triphosphate Anions in Vacuo: Probing the Influence of Charge State on the UV Photophysics of Adenine

Journal:	*The Journal of Physical Chemistry*
Manuscript ID	jp-2017-03435v.R1
Manuscript Type:	Article
Date Submitted by the Author:	n/a
Complete List of Authors:	Cercola, Rosaria; University of York, Department of Chemistry Matthews, Edward; University of York, Chemistry Dessent, Caroline; University of York, Department of Chemistry

Photoexcitation of Adenosine-5'-Triphosphate Anions in Vacuo: Probing the Influence of Charge State on the UV Photophysics of Adenine

Rosaria Cercola, Edward Matthews and Caroline E. H. Dessent*

Department of Chemistry, University of York, Heslington, York, YO10 5DD, UK.

ABSTRACT

We report the first UV laser photodissociation spectra (4.0-5.8 eV) of gas-phase deprotonated adenosine 5'-triphosphate, diphosphate and monophosphate anions. The photodepletion spectra of these anions display strong absorption bands across the region of 4.6-5.2 eV, consistent with excitation of a primarily adenine-centred π-π* transition. The spectra appear insensitive to the charge of the species (i.e. the spectrum of $[ATP-2H]^{2-}$ closely resembles that of $[ATP-H]^-$), while the spectral profile is affected to a greater extent by the variation of the molecular structure, i.e. the $[AMP-H]^-$ and $[ADP-H]^-$ photodepletion spectra display similar profiles while the $[ATP-H]^-$ spectrum is distinctive. The photodepletion cross-section also decreases for the ATP anions compared to both the AMP and ADP anions, reflecting a high intrinsic photostability of ATP versus both AMP and ADP. A range of photofragments are produced across the 4.0-5.8 eV spectral range for all of the ATP analogues studied. These fragments are primarily associated with fragmentation on the ground-state electronic surface, indicative of a statistical decay process where ultrafast decay is followed by ergodic dissociation. However, while the photofragments observed following photoexcitation of the monoanionic species, $[AMP-H]^-$ to $[ADP-H]^-$ to $[ATP-H]^-$ are entirely consistent with statistical decay, an additional group of photofragments are observed for the dianionic species, $[ADP-2H]^{2-}$ and $[ATP-2H]^{2-}$, that we associate with electron detachment, and subsequent fragmentation of the resulting electron-detached photofragment. TDDFT calculations are presented to support the interpretation of the experimental data, and confirm that the electronic structure of the adenine moiety is relatively unperturbed by varying the overall charge.

* Corresponding author

1. Introduction

The ultrafast photophysical and photochemical processes that occur in DNA following UV excitation have been the subject of intense investigation, since the absorption of UV radiation can lead to biological damage, including mutations and strand breaks.[1,2] Such photodamage processes display low quantum yields, however, due to the operation of non-radiative decay mechanisms that enable nucleobases to dissipate the harmful electronic excitation into more benign thermal energy. Much effort has been expended into obtaining a molecular-level understanding of these processes, with a particular focus both experimentally and theoretically on adenine.[3-8]

Gas-phase experiments provide a useful complement to solution-phase measurements, since they can often provide more detail and allow a more straightforward comparison between experiment and theory. Instrumental developments linking electrospray ionisation with UV laser spectroscopy provided a route to extend earlier gas-phase experiments on the simple nucleobases to the more complex oligonucleotides.[9-16] For example, Marcum et al. have used photodissociation spectroscopy to study photodamage in isolated mononucleotides,[10] and Chatterley et al. have used time-resolved photoelectron imaging spectroscopy to explore the ultrafast dynamics of the nucleotide and selected oligonucleotides of adenine.[11] One of the key questions raised by these studies is the extent to which the native negative charge carried by a deprotonated oligonucleotide can affect the intrinsic photophysics and photochemistry of the adenine moiety.

In this work, we present the first gas-phase UV laser photodissociation spectra of a series of deprotonated anions of adenosine 5'-triphosphate (ATP), diphosphate (ADP) and monophosphate (AMP), illustrated in Scheme 1. Adenosine 5'-triphosphate plays the central role in the storage and distribution of energy in cells, and is also of key importance in signal

transduction via the production of 3',5'-cyclic adenosine monophosphate (cAMP).[17] Although ATP is an important biological molecule, our focus in this work is on using the ATP/ADP/AMP series of molecules as a facile test system to investigate the effect of changing the charge state on the UV photochemistry of adenine nucleobase. The question of how an adjacent negative charge influences the UV photophysics of a nucleobase is also of fundamental relevance to the correct interpretation of a number of recent laser experiments on molecular clusters that include nucleobases, e.g. iodide ion-nucleobase clusters and platinum complex anion-nucleobase clusters.[18-21] Importantly, Compagnon et al. identified a strong bathochromic shift in the electronic excitation of tryptophan on going to the monoanionic deprotonated species.[22] This shift was attributed to the impact of an adjacent excess negative charge on the tryptophan chromophore. The experiments performed here allow us to investigate whether this is a general phenomenon or an effect specific to the tryptophan system.

2. Methods

Gas-phase UV photodepletion and photodissociation experiments were conducted in an AmaZon quadrupole ion-trap mass spectrometer, which was modified for conducting laser experiments as described in detail previously.[20] UV photons were produced by an Nd:YAG (10 Hz, Surelite) pumped OPO (Horizon) laser, giving ~1 mJ across the range 215-345 nm. The laser step size employed was 1 nm. Photofragmentation experiments were run with an ion accumulation time of 100 ms. A fragmentation time of 100 ms was employed, so that each mass-selected ion packet interacted with one laser pulse. Moreover, due to the fact that the ions are continually circulating within the ion cloud, the probability of multiphoton excitation of an ion is very low. This was verified by conducting laser power studies across the scanned spectral range, which showed that ion photodepletion was linear with respect to

laser power, consistent with single photon absorption. The photodepletion intensity (PD) of the clusters and the photofragment production (PF) have been calculated using equations 1 and 2 and are presented as a function of the photon energy.

$$\text{Photodepletion Intensity} = \frac{\text{Ln}\left(\frac{\text{Int}_{\text{OFF}}}{\text{Int}_{\text{ON}}}\right)}{\lambda \times \text{P}} \qquad [1]$$

$$\text{Photofragmentation Production} = \frac{\left(\frac{\text{Int}_{\text{Frag}}}{\text{Int}_{\text{OFF}}}\right)}{\lambda \times \text{P}} \qquad [2]$$

Where Int_{ON} and Int_{OFF} are the peak intensities with laser on and off, Int_{Frag} is the fragment intensity with laser on, λ is the excitation wavelength (nm) and P is the laser pulse energy (mJ). Equation [1] includes a natural logarithm in line with common practice for calculating photodepletion (See Ref [22]), while no natural logarithm is included in Equation [2]. This practice is adopted because some photofragment intensities can be low, which would lead to unintuitive negative values for photofragment production if a natural logarithm was used. Solution-phase UV absorption spectra (aqueous solution, $3\text{x}10^{-5}$ mol dm^{-3}) were recorded using a Shimadzu 1800 UV spectrophotometer with a 1 cm UV cuvette, using distilled water as a baseline.

Higher-energy collisional dissociation (HCD) was performed to investigate the ground state fragmentation characteristics of the $[\text{AXP-}n\text{H}]^{n-}$ (X = M, D, T and n = 1, 2) anions. An Orbitrap Fusion Tribrid mass spectrometer (Thermo Fisher Scientific) with an ESI source was employed for these experiments, run in the negative ion mode. The HCD fragmentation technique as implemented on the Orbitrap mass spectrometer provides tandem mass spectrometry, similar to triple quadrupole fragmentation.[23] The instrument was operated at a flow rate of 20 μL/min and with the following parameters: spray voltage -2453V; sweep gas flow rate, 0; sheath gas flow rate, 35; aux gas flow rate, 10; ion transfer tube temperature, 325 °C; vaporizer temperature, 150 °C; MS^1 detector, Ion Trap; MS^1 scan range, 50–600; MS^1 maximum injection time, 100 ms; MS^1 automated gain control (AGC) target, 100,000; MS^2

detector, Ion trap; MS^2 AGC target, 100,000; MS^2 maximum injection time, 100, S-lens RF level, 60 V (10 V for the dianions). The HCD collisional energy was varied between 0 and 45 %, and the intensity of the ion in percentage was calculated.

Solutions of ATP (1×10^{-5} mol dm^{-3}) in deionised water were introduced to the mass spectrometer through electrospray ionisation using a nebulising gas pressure of 10.0 psi, an injection rate of 250 μL/hr, a drying gas flow rate of 8.0 L min^{-1}, and a capillary temperature of 180°C. ATP was purchased from Sigma Aldrich and used without purification. We anticipate that the ATP analogues will be deprotonated on the phosphate side chains. This point is discussed further in Ref. 24.

Density functional theory (DFT) was used to calculate vertical detachment energies (VDEs) of the $[AMP-H]^-$, $[ADP-H]^-$, $[ATP-H]^-$, $[ADP-2H]^{2-}$ and $[ATP-2H]^{2-}$ anions. Calculations were performed at the M06-2X/6-311++G** level as implemented in Gaussian 09.[25] The method used to obtain the optimized structures is described in detail in the Supporting Information.

3. Results and Discussion

i. Photodepletion Spectra

The photodepletion spectra of the $[AMP-H]^-$, $[ADP-H]^-$, $[ATP-H]^-$, $[ADP-2H]^{2-}$ and $[ATP-2H]^{2-}$ anions are displayed in Figure 1. (We label these species as $[AXP-nH]^{n-}$ where X = M, D, T and n = 1,2.) These spectra can be considered as gas-phase absorption spectra, in the limit where fluorescence is not a significant decay channel following electronic excitation.[26] The spectra are all similar in that they display broad absorption features between ~4.6-5.2 eV, with the photodepletion cross section remaining considerable (or increasing) towards the high-energy limit of the scans. We note that the photodepletion intensity of ATP is markedly

smaller than the photodepletion intensities of AMP and ADP, indicating that the ATP anions are inherently more photostable than the AMP and ADP analogues. To test that the photodepletion spectra correspond to single-photon absorption spectra, laser-power dependent photodepletion measurements (0.5 to 1.5 mJ) were conducted at 4.9 eV, close to the maxima of the broad absorption maxima bands. Figure 2 displays these power-dependent measurements, which are linear across this range, confirming that photoexcitation under the experimental conditions employed here (100 ms fragmentation time, 1.0 mJ pulse energy) is a one-photon process.

Figure 3 presents the aqueous absorption spectra of solutions of ATP recorded at a range of pHs (between 1 and 12) for comparison with the gas-phase spectra. Despite the change in pH, these solution-phase absorption spectra are remarkably similar, displaying a prominent absorption between 4.6 and 5.2 eV (λ_{max}~4.75 eV), followed by a strongly increasing absorption profile towards the high-energy limit of the scan. The λ_{max}~4.75 eV absorption band has been associated with the π-π^* transition centred on the adenine moiety,[6,7,27,28] and this feature dominates the spectra irrespective of the fact that the various ATP solutions will contain mixtures of differentially deprotonated ATP, ADP and AMP species.[29]

Returning to the gas-phase photodepletion spectra (Figure 1), we therefore assign the broad absorptions observed between ~4.6-5.2 eV as arising from the same, predominantly adenine-centred π-π^* transition that appears with λ_{max}~4.75 eV for the solution-phase ATP species.[29] It is evident that this absorption is relatively insensitive to whether the species carries a single or a double negative charge (e.g. the $[ATP\text{-}H]^-$ spectrum closely resembles that of the $[ATP\text{-}2H]^{2-}$ spectrum). Although the photodepletion spectra of all of the $[AXP\text{-}nH]^{n-}$ anions are broadly similar, the spectra are modified by whether the adenosine species carries a mono-, di- or triphosphate tail. This is most evident for the $[ATP\text{-}nH]^{n-}$ species which have spectra

that display a considerably more sharply increasing absorption profile towards high energy compared to the ADP and AMP species. We note that the strong absorption towards the high-energy tail we observe here mirrors the spectral profile of solution-phase ATP (Figure 3).

It is instructive to consider where the photodepletion spectra appear with respect to the electron detachment energies of the $[AXP\text{-}nH]^{n-}$ anions. Photoelectron spectra of the dianionic species have been recorded by Schinle at al.,[30] but since we have no experimental electron affinities for the monoanions, we calculated electron affinities for all of the species studied here and use them as a complete set of values, where relative values should be reliable. These calculated VDEs are included in Table 1. For the monoanions, $[AXP\text{-}H]^-$, the VDEs all lie above the high-energy limit of the scans, indicating that the electronic transitions observed in Figures 1a-1c lie well below the electron detachment continuum. The situation is slightly different for the dianionic species, $[ADP\text{-}2H]^{2-}$ and $[ATP\text{-}2H]^{2-}$, which we predict to have vertical detachment energies of 3.10 and 4.11 eV. However, the threshold for electron detachment is only reached around ~5.3 and 6.0 eV,[30] respectively, when the repulsive coulomb barrier (RCB) for electron detachment is exceeded.[31,32] Therefore, the dianion photodepletion spectra also lie predominantly below the electron detachment continuum, although there is likely to be some photodetachment below these energies associated with electron tunnelling through the RCB.[31,32]

While the overall spectral profile is similar for all of the $[AXP\text{-}nH]^{n-}$ anions, it is evident that there are differences between the spectral profiles. One prominent example of this is the way that the ATP species (Figures 1c and 1e) display a much more strongly increasing photodepletion cross-section to high-energy. To further explore the differences in the photodepletion spectra and the decay pathways that follow photoexcitation,[33] we will

investigate the spectral profile for the photofragment production spectra that accompany the photodepletion spectra in Section 3iii.

ii. Collision-Induced Dissociation

Higher-energy collisional dissociation (HCD) was performed for the series of $[AXP\text{-}nH]^{n-}$ (X = M, D, T and n = 1, 2) anions to fully characterise their ground electronic-state fragmentation behaviour. The HCD fragmentation curves are displayed in Figure 4. Inspection of the fragmentation curves shows that a number of larger molecular fragments are produced only over a limited energy range, with fragmentation into smaller ionic species becoming dominant at higher collision energies. One example is provided by the $[ADP\text{-}H]^-$ anion (Figure 4b) which fragments with production of $[cAMP\text{-}H]^-$ only between 10-35% HCD, and also the corresponding dianion, $[ADP\text{-}2H]^{2-}$ (Figure 4d) which produces the $[AMP\text{-}H]^-$ fragment only between 0-28% HCD. Although there have been previous collision-induced dissociation (CID) measurements conducted on the $[ATP\text{-}2H]^{2-}$ and $[ADP\text{-}2H]^{2-}$ dianions (low-energy CID),[24] and the $[AMP\text{-}H]^-$ monoanion (higher-energy CID),[34] this is the first time that a comparable set of CID profiles have been obtained for the $[AXP\text{-}nH]^{n-}$ series.

In the previous CID measurements of the $[AMP\text{-}H]^-$ anion by Ho and Kebarle,[34] an absolute measurement of centre of mass collision energy was obtained through absolute calibration. Comparison of the current results for $[AMP\text{-}H]^-$ (Figure 4a) with these earlier measurements,[34] allows us to obtain an approximate calibration of the HCD fragmentation curves presented in Figure 4. From this comparison, it appears that the 4-6 eV energy range (i.e. the photon range employed in our laser experiments, and hence the maximum amount of energy that would be available to fragment the ground state surface anions) corresponds to the 20-38% range on the HCD fragmentation plots (Figure 4).

iii. Photofragmentation Mass Spectra

Figure 5 displays the photofragment mass spectra obtained for photoexcitation of the $[AXP-nH]^{n-}$ anions at 4.9 eV, close to the peaks of the photodepletion spectra. (A list of the prominent photofragments observed is included in Table 2.) Photofragments associated with fission of the phosphate side chain are common, *e.g.* PO_3^- and $HP_2O_6^-$. For $[ATP-2H]^{2-}$ (Figure 5e), the PO_3^- photofragment is observed with the accompanying monoanion in photofragmentation of the dianionic species, consistent with a photoinduced ionic fragmentation process,[10,23,32] e.g.

$$[ATP-2H]^{2-} + h\nu \rightarrow PO_3^- + [ADP-H]^- \quad [3]$$

Deprotonated adenine, $[A-H]^-$ is seen as a prominent photofragment for $[AMP-H]^-$, $[ADP-H]^-$, and $[ADP-2H]^{2-}$ (Figures 5a, 5b and 5d). It should be noted that although we refer to this fragment as deprotonated adenine, it could equivalently be described as A^-, i.e. the anionic nucleobase formed upon rupture of the CN glycosidic bond.[34] The $[A-H]^-$ anion has been observed as a stable photofragment in several recent studies of clusters that include adenine.[20] Intriguingly, $[A-H]^-$ it is not observed as a significant intensity photofragment for either of the ATP anions (Figures 5c and 5e). Electron detachment is observed for both of the dianionic species (Figures 5d and 5e), e.g.

$$[ADP-2H]^{2-} + h\nu \rightarrow [ADP-2H]^- + e^- \quad [4]$$

This is despite the fact that this photoexcitation energy, although greater than the adiabatic electron affinity, is still considerably below the electron detachment onsets associated with exceeding the RCB (see Section 3i).

As described in Section 3ii, a series of HCD experiments were conducted on the $[AXP\text{-}nH]^{n-}$ anions to establish which ionic fragments are produced on the ground state surface following collisional excitation. Table 2 presents a comparison of the major photofragments obtained with a photoexcitation energy of 4.9 eV, along with the anionic fragments obtained with an HCD centre-of-mass collision energy of 24%, i.e. a similar energy to the laser photon energy. For systems where photoexcitation is followed by rapid decay back to the ground-state surface and subsequent ergodic (statistical) dissociation, the photofragments are expected to mirror the HCD fragments produced when an amount of energy equivalent to the photon energy is deposited in the ground-state system.[9,10] Inspection of Table 2 reveals that the major 4.9 eV photofragments largely mirror the major 24% HCD fragments, consistent with a predominantly statistical decay process. For the dianionic systems, all the fragments observed in the HCD experiment are seen as photofragments, along with a small number of additional photofragment species e.g $[cADP]^-$ from $[ADP\text{-}2H]^{2-}$.[35] It appears that photofragmentation represents a slightly softer fragmentation process than HCD, since larger fragments such as $[cADP]^-$ can be seen in photofragmentation but are absent in HCD, presumably due to secondary fragmentation of primary CID fragments that are produced with high internal energy. We note that while similar sets of photofragments and HCD fragments are observed for all of the ATP analogues, the relative intensities (of a set of fragments produced by a single $[AXP\text{-}nH]^{n-}$ species in photofragments *versus* HCD) vary more on going to longer phosphate chain length and to higher charge. For the dianionic systems, this observation can largely be attributed to the electron-detachment decay pathway of a multiply-charged anion being accessed via photoexcitation in addition to adenine-centred π-π^* transitions.

The observation that all of the $[AXP\text{-}nH]^{n-}$ anions produce a group of photofragments that mirrors the CID fragments indicates that each of the $[AXP\text{-}nH]^{n-}$ anions follow broadly

similar decay pathways following photoexcitation at 4.9 eV, irrespective of the charge state or the phosphate chain length. This picture is consistent with the photodepletion spectra discussed above, and with the known photophysics of adenine (i.e. ultrafast decay with subsequent ergodic dissociation),[5-9] and thus again indicates that the adenine moiety is largely unaffected across the $[AXP\text{-}nH]^{n-}$ series.

Table 3 compares the photofragment mass spectra observed following photoexcitation at 5.6 eV with the ionic fragments produced upon HCD at 36% collision energy. The propensity for production of lower mass fragments (e.g. PO_3^- and $H_2PO_4^-$) can be seen to increase, as both the laser excitation energy and the collision excitation energy increase. As for the 4.9 eV photoexcitation data presented above, similar fragmentation patterns are observed for both laser excitation and collisional excitation, indicating that a largely ergodic dissociation process is also occurring at high-energy, along with the additional multiply-charged anion photofragment pathways.

iv. Photofragment Action Spectra

Figure 6 displays the photofragment action spectra (4.0-5.8 eV) for production of some photofragments of the $[AXP\text{-}nH]^{n-}$ anions. For the $[AMP\text{-}H]^-$ anion (Figure 6a), the major photofragments PO_3^- and $H_2PO_4^-$ are produced smoothly through the main photodepletion band (λ_{max}~5.0 eV), and then increase strongly in intensity towards the high-energy tail of the spectrum. The $[A\text{-}H]^-$ anion displays a similar profile, although production of this photofragment peaks slightly lower in energy (~4.85 eV), and increases less strongly towards the high-energy limit. This difference in the band shapes for production of the $[A\text{-}H]^-$ photofragment compared to the PO_3^- and $H_2PO_4^-$ pair of photofragments explains the shape of

the overall photodepletion spectrum (Figure 1a), where a step is visible at ~4.85 eV associated with production of the $[A-H]^-$ photofragment peaking at this excitation energy.

Figure 6b displays the photofragment action spectra for $[ADP-H]^-$. This set of photofragment action spectra show the advantage of recording the photofragment action spectra, compared to just the photodepletion spectrum (Figure 1b), since they clearly reveal that two distinct fragmentation processes occur across the spectral region investigated. Production of the $[cAMP-H]^-$ photofragment peaks strongly at 4.7 eV, dropping to zero above 5.6 eV, while the $[A-H]^-$ photofragment peaks close to 5.25 eV, probably due to the $[cAMP-H]^-$ fragmenting into $[A-H]^-$ with maximum cross section around this energy The distinctive profile of the $[cAMP-H]^-$ photofragment between 4.7-5.6 eV closely mirrors the production of this ion at only a limited range of HCD energies (Figure 4b), and is strong evidence that this photofragment is produced through a statistical decay process. The $HP_2O_6^-$ photofragment appears to be produced concurrent with both of the $[cAMP-H]^-$ and $[A-H]^-$ photofragments.

$HP_2O_6^-$ and $[cADP]^-$ are observed as the major photofragments for the $[ATP-H]^-$ monoanion (Figure 6c). Both photofragments are produced with identical profiles across the 4.0-5.0 eV region, although the $[cADP]^-$ fragment is produced much less strongly than the $HP_2O_6^-$ fragment above 5.0 eV. This behaviour again mirrors the HCD results for this anion (Figure 4c), with production of $HP_2O_6^-$ increasing towards high collision energy, while the intensity of the $[cADP]^-$ fragment tails off, again probably due to the $[cADP]^-$ fragmenting into $HP_2O_6^-$.

Figure 6d displays the photofragment action spectra for the fragments produced from the $[ADP-2H]^{2-}$ dianion. These spectra show similar profiles, although the PO_3^- fragment and the $H_3P_2O_7^-$ both show an increasing production profile towards high energy. The $H_3P_2O_7^-$ and

$[cADP]^-$ fragments also display a similar profile, with an onset around 4.3 eV and a maximum around close to the maximum of the electron detachment fragment, $[ADP\text{-}2H]^-$.

It is intriguing that the $[ATP\text{-}2H]^-$ electron detachment fragment is produced so strongly through the 4.4-5.2 eV region (Figure 6e), since this energy is considerably below the expected electron detachment threshold (Section 3i). It appears that the excited state accessed in this region is able to couple efficiently to an electron detachment coordinate that circumvents the repulsive coulomb barrier. This phenomenon is not unique to the $[ATP\text{-}2H]^{2-}$ dianion, since in a recent photoelectron spectroscopy study of $Pt(CN)_4^{2-}$·nucleobase clusters, delayed electron detachment signals were observed when the adenine cluster was irradiated at 266 nm (4.66 eV). This appeared to be due to excitation of long-lived adenine-centred excited states that can effectively couple to the electron detachment continuum. [36]

To summarize, the $[AXP\text{-}nH]^{n-}$ anions produce a range of different photofragments across the 4.0-5.8 eV range. In general, production of the smaller fragment ions, e.g. $H_2PO_4^-$, PO_3^- and $HP_2O_6^-$, increases towards the high-energy region of the spectrum, and the overall patterns for production of photofragments as a function of excitation energy mirrors those observed using high-energy collisional excitation. The energy redistribution process involved in ergodic dissociation following fast internal conversion back to the ground state may not exactly match the energy transfer (and subsequent energy redistribution) that occurs upon higher-energy collision induced dissociation. However, the close relationship between photofragments and collisional fragments observed here, strongly indicates that the $[AXP\text{-}nH]^{n-}$ anions do undergo rapid conversion back to the electronic ground state following photoexcitation, as would be expected for a system with a largely adenine-centred chromophore.

v. Time-dependent density functional theory calculations

To gain further insight into the nature of the electronic excitations involved in photoexcitation of the $[AXP\text{-}nH]^{n-}$ anions across the 4-6 eV range, time-dependent density functional theory (TDDFT) calculations were performed. Full details of these calculations, along with the full results are presented in Section S3 of the supporting information. The TDDFT calculations were able to accurately predict the general form of the photodepletion spectra, with each anion displaying a broad absorption between 4.4-5.6 eV, followed by an increasing absorption profile to high photon energy. In general, the main electronic transitions originated from orbitals with electron density on both the adenine and the phosphate group(s), indicating extensive orbital mixing across the molecular framework. The dominant transition in the region of the maximum (~5.0 eV) of the 4.4-5.6 eV absorption band was found to be associated with the expected π-π^* transition on adenine. n-$\pi^*$and σ-based transitions are also common, particularly in the high-energy excitation regions.

Comparing the calculated spectra and the component electronic excitations for pairs of anions with the same molecular framework but different excess negative charges (e.g. $[ATP\text{-}2H]^-$ versus $[ATP\text{-}2H]^{2-}$), indicates that there is little change in the excitation energies or extinction coefficients of the main electronic excitations with variation in excess charge. For the adenine-centred chromophoric molecules studied here, we therefore conclude that there is no substantial bathochromic shift associated with negative charges existing in close proximity to the nucleobase.[22]

4. Further Discussion

Nielsen *et al.* studied the photodestruction of $[AMP-H]^-$ at 266 nm (4.66 eV),[9] and found that the excited state lifetime was 16μs, with the major part of photofragmentation occurring by an ergodic process. The photofragment identities associated with excited state decay could not be identified in that experiment due to instrumental limitations. However, the set of photofragments of $[AMP-H]^-$ observed in the current study (i.e. PO_3^-, $H_2PO_4^-$ and $[A-H]^-$) with 4.9 eV excitation are entirely consistent with photofragmentation occurring *via* an ergodic process since the photofragments are identical to the major HCD fragments observed with a similar collisional excitation energy.

The ultrafast dynamics of adenine following 4.66 eV photoexcitation was also investigated by Verlet and co-workers via time-resolved photoelectron imaging of the deprotonated 3'-deoxy-adenosine-5'monophosphate nucleotide, and its di- and trinucleotides.[11,12] These experiments revealed that the dynamics of the base are relatively insensitive to the surrounding environment, and led to the conclusion that the decay mechanism primarily involves internal conversion from the initially populated $^1\pi$-π^* states to the ground states. These results again mirror the results found in this study, across the 4.4-5.2 eV absorption band. In another related work, Weber and co-workers studied the photodissociation spectroscopy of a series of deprotonated nucleotides, including deprotonated 2'-deoxy-adenosine-5'-monophosphate.[10] Their results are again largely consistent a photodecay mechanism that involves rapid electronic relaxation followed by unimolecular fragmentation on the vibrationally hot ground-state surface.

The results presented herein complement these earlier results, since they demonstrate how the ATP anions appear to share much of the photophysical properties that were observed previously. Photoexcitation across the 4-5.8 eV region appears to largely follow the expected adenine-centred excitation followed by rapid relaxation via a conical intersection and subsequent ground-state statistical decay. The TDDFT calculations provide a picture of

electronic excitations that contain significant adenine-centred π-π* character, but are delocalized across the entire molecular framework, possibly facilitating statistical decay. One interesting point of note in comparing the ATP experiments conducted with the deoxy-nucleotides studied by Verlet and Weber is that the presence of two OH groups on the ribose in the ATP analogues, means that the anions are able to maintain a hydrogen-bond network across the molecular ion (see Section S1 of the supporting information for calculated geometric structures). Such molecular structures have recently been identified to facilitate ultrafast decay mechanisms,[7] and appear likely to be a key factor in the overall photostability of ATP.

It is interesting to consider the results of the current work in the context of the photodetachment study of the tryptophan anion conducted by Compagnon and co-workers.[22] They found via experiment and TDDFT calculations that the tryptophan chromophore was sensitive to the presence of the excess negative charge in the anion, resulting in substantial bathochromism of the main electronic excitations of up to 25 nm. No such dramatic shift is observed here on going from the monanionic to dianionic species, either experimentally or in the TDDFT calculations. It seems possible that this differing behaviour can be traced to the very different geometric arrangements of the chromophores and excess charges in the tryptophan anion compared to the $[AXP\text{-}nH]^{n-}$ anions. Alternatively, it may be that the electronic excitations of the adenine chromophore studied here are particularly insensitive to environmental changes,[11,12] including excess charge. Nonetheless, the considerable differences in bathochromism between deprotonated tryptophan and ATP are notable. Further investigation of a broader range of molecular anions where excess charge is located at a distance from a chromophore are desirable to clarify the generality of excess-charge induced electronic transition shifts.

5. CONCLUDING REMARKS

The photofragmentation measurements conducted on the $[AXP\text{-}nH]^{n-}$ series of anions indicate that the decay dynamics are consistent with photoexcitation of a largely adenine centred chromophore that undergoes ultrafast decay following photoexcitation. Both the photodepletion spectra and photofragmentation patterns indicate that the adenine moiety within the ATP anions appears to be unaffected by the charge state of the molecular system. This is an important result for clarifying the interpretation of recent experiments that have been conducted on anion-nucleobase clusters such as I^-·uracil and $Pt(CN)_4^{2-}$·adenine.[18,36] In further work, it would be interesting to directly monitor the inferred decay dynamics by probing the production of the various photofragments via ultrafast spectroscopy. Time-resolved photodetachment photoelectron spectroscopy provides a facile approach to such measurements,[37] and could be readily applied to the system studied here.

ASSOCIATED CONTENT

Supporting Information

The Supporting Information is available free of charge on the ACS Publications website at DOI: xxx.

Details of geometry optimization, TD-DFT calculations of the electronic transitions, DFT calculations of the $cADP^-$ anion and photofragment mass spectra (4.7 and 5.6 eV).

AUTHOR INFORMATION

Corresponding author

*Caroline E. H. Dessent. E-mail: caroline.dessent@york.ac.uk

ORCID

Caroline E.H. Dessent: 0000-0003-4944-0413

Notes

The authors declare no competing financial interest.

ACKNOWLEDGEMENTS

We thank the University of York and the Department of Chemistry and the University of York for provision of funds for the Horizon OPO laser system. RC thanks the Department of Chemistry at the University of York for funding via a departmental studentship. We also thank the EPSRC UK NSCCS at Imperial College London for the award of grant CHEM 666.

The York Centre of Excellence in Mass Spectrometry was created thanks to a major capital investment through Science City York, supported by Yorkshire Forward with funds from the Northern Way Initiative, and subsequently received additional support from the EPSRC.

REFERENCES

1. Sanche, L. Low Energy Electron-Driven Damage in Biomolecules. *Eur. Phys. J. D* **2005**, *35*, 367-390.
2. Simons, J. How Do Low-Energy (0.1−2 eV) Electrons Cause DNA-Strand Breaks? *Acc. Chem. Res.* **2006**, *39*, 772-779.
3. Sobolewski, A. L.; Domcke, W. The Chemical Physics of the Photostability of Life. *Europhysics News* **2006**, *37*, 20-23.
4. Roberts, G. M.; Stavros, V. G. The Role of πσ* States in the Photochemistry of Heteroaromatic Biomolecules and Their Subunits: Insights from Gas-Phase Femtosecond Spectroscopy. *Chem. Sci.* **2014**, *5*, 1698-1722.
5. De Camillis, S.; Miles, J.; Alexander, G.; Ghafur, O.; Williams, I. D.; Townsend, D.; Greenwood, J. B. Ultrafast Non-Radiative Decay of Gas-Phase Nucleosides. *Phys. Chem. Chem. Phys.* **2015**, *17*, 23643-23650.
6. Bisgaard, C. Z.; Satzger, H.; Ullrich S.; Stolow, A. Excited-State Dynamics of Isolated DNA Bases: A Case Study of Adenine. *Chem. Phys. Chem.* **2009**, *10*, 101-110.
7. Tuna, D.; Sobolewski, A. L.; Domcke, W. Mechanisms of Ultrafast Excited-State Deactivation in Adenosine. *J. Phys. Chem. A* **2014**, *118*, 122-127.
8. Miyazaki, M.; Kang, H.; Choi, C. M.; Han, N. S.; Song, J. K.; Kim, N. J.; Fujii, M. MODE-Specific Deactivation of Adenine at the Singlet Excited States. *J. Chem. Phys.* **2013**, *139*, 124311.
9. Nielsen, S. B.; Andersen, J. U.; Forster, J. S.; Hvelplund, P.; Liu, B.; Pedersen, U. V.; Tomita, S. Photodestruction of Adenosine 5'-Monophosphate (AMP) Nucleotide Ions in Vacuo: Statistical Versus Nonstatistical Processes. *Phys. Rev. Lett.* **2003**, *91*, 048302.

10. Marcum, J. C.; Halevi A.; Weber, J. M. Photodamage to Isolated Mononucleotides-Photodissociation Spectra and Fragment Channels. *Phys. Chem. Chem. Phys*. **2009**, *11*, 1740-1751.

11. Chatterley, A. S.; West, C. W.; Roberts, G. M.; Stavros, V. G.; Verlet, J. R. R. Mapping the Ultrafast Dynamics of Adenine onto Its Nucleotide and Oligonucleotides by Time-Resolved Photoelectron Imaging. *J. Phys. Chem. Lett.* **2014**, *5*, 843-848.

12. Chatterley, A. S.; West, C. W.; Stavros, V. G.; Verlet, J. R. R. Time-Resolved Photoelectron Imaging of the Isolated Deprotonated Nucleotides. *Chem. Sci*. **2014,** *5*, 3963-3975.

13. Berdakin, M.; Férau, G.; Dedonder-Lardeux, C.; Jouvet, C.; Pino, G. A. Excited States of Protonated DNA/RNA Bases. *Phys. Chem. Chem. Phys.* **2014**, *16*, 10643-10650.

14. Pedersen, S. Ø.; Støchkel, K.; Byskov, C. S.; Baggesen L. M.; Nielsen, S. B. Gas-Phase Spectroscopy of Protonated Adenine, Adenosine 5'-Monophosphate and Monohydrated Ions. *Phys. Chem. Chem. Phys*. **2013**, *15*, 19748-19752.

15. Milosavljević, A. R.; Cerovski, V. Z.; Canon, F.; Ranković, M. L.; Škoro, N.; Nahon, L.; Giuliani A. Energy-Dependent UV Photodissociation of Gas-Phase Adenosine Monophosphate Nucleotide Ions: The Role of a Single Solvent Molecule. *J. Phys. Chem. Lett.* **2014**, *5*, 1994-1999.

16. Yang, X.; Wang, X. B.; Vorpagel, E. R.; Wang, L. S. Direct Experimental Observation of the Low Ionization Potentials of Guanine in Free Oligonucleotides by Using Photoelectron Spectroscopy. *Proc. Natl. Acad. Sci. U. S. A.* **2004**, *101*, 17588-17592.

17. Rahman, N.; Buck, J.; Levin, L.R. pH Sensing Via Bicarbonate-Regulated "Soluble" Adenylyl Cyclase (sAC). *Front. Physiol*. **2013**, *4*, 343.

18. Li, W. L.; Kunin, A.; Matthews, E.; Yoshikawa, N.; Dessent, C. E. H.; Neumark, D. M. Photodissociation Dynamics of the Iodide-Uracil (I-U) Complex. *J. Chem. Phys.* **2016**, *145*, 044319.

19. Stephansen, A. B.; King, S. B.; Yokoi, Y.; Minoshima, Y.; Li, W. L.; Kunin, A.; Takayanagi, T.; Neumark, D. M. Dynamics of Dipole- and Valence Bound Anions in Iodide-Adenine Binary Complexes: A Time-Resolved Photoelectron Imaging and Quantum Mechanical Investigation. *J. Chem. Phys.* **2015**, *143*, 104308.

20. Matthews, E.; Sen A.; Yoshikawa, N.; Bergström, E.; Dessent, C. E. H. UV Laser Photoactivation of Hexachloroplatinate Bound to Individual Nucleobases in Vacuo as Molecular Level Probes of a Model Photopharmaceutical. *Phys. Chem. Chem. Phys.* **2016**, *18*, 15143-15152.

21. Sen, A.; Dessent, C. E. H. Mapping the UV Photophysics of Platinum Metal Complexes Bound to Nucleobases: Laser Spectroscopy of Isolated Uracil·$Pt(CN)_4^{2-}$ and Uracil·$Pt(CN)_6^{2-}$ Complexes. *J. Phys. Chem. Lett.* **2014**, *5*, 3281-3285.

22. Compagnon, I.; Allouche, A. R; Bertorelle, F.; Antoine R.; Dugourd, P. Photodetachment of Tryptophan Anion: An Optical Probe of Remote Electron. *Phys. Chem. Chem. Phys.* **2010**, *12*, 3399-3403.

23. Olsen, J. V.; Macek, B.; Lange, O.; Makarov, A.; Horning, S.; Mann, M. Higher-Energy C-Trap Dissociation for Peptide Modification Analysis. *Nat. Methods*, **2007**, *9*, 709-712.

24. Burke, R. M.; Pearce, J. K.; Boxford, W. E.; Bruckmann, A.; Dessent, C. E. H. Stabilization of Excess Charge in Isolated Adenosine 5'-Triphosphate and Adenosine 5'- Diphosphate Multiply and Singly Charged Anions. *J. Phys. Chem. A* **2005**, *109*, 9775-9785.

25. Frisch, M. J.; Trucks, G. W.; Schlegel, H. B.; Scuseria, G. E.; Robb, M. A.; Cheeseman, J. R.; Scalmani, G.; Barone, V.; Mennucci, B.; Petersson, G. A., et al. Gaussian 09, Revision D.1; Gaussian, Inc.: Wallingford, CT, 2009.

26. Wellman, S. M. J.; Jockusch, R. A. Moving in on the Action: An Experimental Comparison of Fluorescence Excitation and Photodissociation Action Spectroscopy. *J. Phys. Chem. A* **2015**, *119*, 6333–6338.

27. Improta, R.; Santoro, F.; Blancafort, L. Quantum Mechanical Studies on the Photophysics and the Photochemistry of Nucleic Acids and Nucleobases. *Chem. Rev.* **2016**, *116*, 3540-3593.

28. Clark, L. B.; Peschel, G. G.; Tinoco, I. Vapor Spectra and Heats of Vaporization of Some Purine and Pyrimidine Bases. *J. Phys. Chem.* **1965**, *69*, 3615-3618.

29. Bock, R. M.; Ling, N. S.; Morell S. A.; Lipton, S. A. Ultraviolet Absorption Spectra of Adenosine-5'-Triphosphate and Related 5'-Ribonucleotides. *Arch. Biochem. Biophys.* **1956**, *62*, 253-264.

30. Schinle, F.; Crider, P. E.; Vonderach, M.; Weis, P.; Hampe, O.; Kappes, M. M. Spectroscopic and Theoretical Investigations of Adenosine 5'-Diphosphate and Adenosine 5'-Triphosphate Dianions in the Gas Phase. *Phys. Chem. Chem. Phys.* **2013**, *15*, 6640-6650.

31. Wang, X. B.; Wang L. S. Photoelectron Spectroscopy of Multiply Charged Anions. *Annu. Rev. Phys. Chem.* **2009**, *60*, 105-126.

32. Boxford, W. E.; Pearce, J. K.; Dessent, C. E. H. Ionic Fragmentation versus Electron Detachment in Isolated Transition Metal Complex Dianions. *Chem. Phys. Lett.* **2004**, *399*, 465-470.

33. Matthews, E.; Dessent, C. E. H. Locating the Proton in Nicotinamide Protomers via Low-Resolution UV Action Spectroscopy of Electrosprayed Solutions. *J. Phys. Chem. A* **2016**, *120*, 9209-9216.

34. Ho, Y.; Kebarle, P. Studies of the Dissociation Mechanisms of Deprotonated Mononucleotides by Energy Resolved Collision-Induced Dissociation. *Int. J. Mass Spectrom.* **1997**, *165-166*, 433-455.

35. The $[cADP]^-$ is a fragment that is common between the $[ADP-2H]^{2-}$, $[ADP-H]^-$ and $[ATP-H]^-$ anions, and is associated with loss of OH^-, H_2O and H_3PO_4, respectively. DFT calculations were conducted to investigate the structure of this cADP unit (Supporting Information) and predict a stable cyclic ADP structure.

36. Sen, A.; Hou, G. L.; Wang X. B.; Dessent C. E. H. Electron Detachment as a Probe of Intrinsic Nucleobase Dynamics in Dianion-Nucleobase Clusters: Photoelectron Spectroscopy of the Platinum II Cyanide Dianion Bound to Uracil, Thymine, Cytosine, and Adenine. *J. Phys. Chem. B* **2015**, *119*, 11626-11631.

37. Anstöter, C. S.; Bull, J. N.; Verlet, J. R. R. Ultrafast Dynamics of Temporary Anions Probed Through the Prism of Photodetachment. *Int. Rev. Phys. Chem.* **2016**, *35*, 509-538.

TABLES

Table 1: M06-2X/6-311++G calculated vertical detachment energies (VDEs) and electron detachment onset energies of the [AXP- *n*H]$^{n-}$ (*n* = 1,2) anions.[c]**

Ion	Calculated VDEs (eV) [a]	Electron Detachment Onset Energies (eV) [b]
$[AMP-H]^-$	6.04	
$[ADP-H]^-$	6.17	
$[ATP-H]^-$	6.24	
$[ADP-2H]^{2-}$	3.10	5.3
$[ATP-2H]^{2-}$	4.11	6.0

[a] Not zero point energy corrected.
[b] Calculated VDEs combined with the experimental RCB from Ref 24.
[c] See Section S1 of SI for details.

Table 2: Photofragments observed following photoexcitation at 4.9 eV and higher-energy collisional dissociation (HCD) fragments obtained at 24% collisional energy for the $[AXP\text{-}nH]^{n-}$ (n = 1,2) anions.[a]

Parent ion	Photofragments (4.9 eV)	HCD fragments (24%)
$[AMP\text{-}H]^-$	$PO_3^- \approx H_2PO_4^-$, $[A\text{-}H]^-$, $[AMP\text{-}H\text{-}A]^-$	PO_3^-, $H_2PO_4^-$, $[AMP\text{-}H\text{-}A]^-$ $[A\text{-}H]^-$
$[ADP\text{-}H]^-$	$[A\text{-}H]^-$, $[cAMP\text{-}H]^-$, $HP_2O_6^-$, $[cADP]^-$ $\approx PO_3^-$, $[ADP\text{-}H\text{-}A]^-$, $[ADP\text{-}H\text{-}A\text{-}H_2O]^-$	$[cAMP\text{-}H]^-$, $[cADP]^-$, $HP_2O_6^-$, $[A\text{-}H]^-$, $[ADP\text{-}H\text{-}A\text{-}H_2O]^-$, PO_3^-, $[ADP\text{-}H\text{-}A]^-$
$[ATP\text{-}H]^-$	$HP_2O_6^- \approx [cADP]^-$, $H_3P_2O_7^-$	$[cADP]^-$, $HP_2O_6^-$, $H_3P_2O_7^-$
$[ADP\text{-}2H]^{2-}$	$H_3P_2O_7^-$, $[A\text{-}H]^- \approx [cADP]^-$, $HP_2O_6^-$, $H_2PO_4^-$, P O_3^-, $[ADP\text{-}2H]^-$, $[AMP\text{-}H]^-$	PO_3^-, $[A\text{-}H]^-$, $H_2PO_4^-$, $[AMP\text{-}H]^-$
$[ATP\text{-}2H]^{2-}$	$[ADP\text{-}H]^- \approx HP_2O_6^-$, $[ATP\text{-}2H]^-$, $H_4P_3O_{10}^-$, $[ATP\text{-}2H\text{-}A]^-$, PO_3^-, $[cAMP\text{-}H]^-$, $[A\text{-}H]^-$	PO_3^-, $[ADP\text{-}H]^-$, $HP_2O_6^-$, $[A\text{-}H]^-$, $[cAMP\text{-}H]^-$

[a] Photofragments and HCD fragments are listed in order of decreasing intensity.

Table 3: Photofragments observed following photoexcitation at 5.6 eV and higher-energy collisional dissociation (HCD) fragments obtained at 36% collisional energy for the $[AXP\text{-}nH]^{n-}$ (n = 1,2) anions.[a]

Parent ion	Photofragments (5.6 eV)	HCD fragments (36%)
$[AMP\text{-}H]^-$	$PO_3^- \approx H_2PO_4^-$, $[A\text{-}H]^-$	PO_3^-, $H_2PO_4^-$, $[A\text{-}H]^-$
$[ADP\text{-}H]^-$	$[A\text{-}H]^-$, $HP_2O_6^-$, $[ADP\text{-}H\text{-}A\text{-}H_2O]^-$, PO_3^-	$HP_2O_6^-$, $[A\text{-}H]^-$, $[ADP\text{-}H\text{-}A\text{-}H_2O]^-$, PO_3^-
$[ATP\text{-}H]^-$	$HP_2O_6^-$, $[cADP]^-$, $H_3P_2O_7^-$, $[ADP\text{-}H\text{-}A\text{-}H_2O]^-$	$HP_2O_6^-$, $[cADP]^-$, $[ADP\text{-}H]^-$, $[ADP\text{-}H\text{-}A\text{-}H_2O]^-$, $H_3P_2O_7^-$
$[ADP\text{-}2H]^{2-}$	$[cADP]^- \approx H_3P_2O_7^-$, $[A\text{-}H]^-$, PO_3^-, $H_2PO_4^-$ $[ADP\text{-}2H]^-$	PO_3^-, $[A\text{-}H]^-$, $H_2PO_4^-$
$[ATP\text{-}2H]^{2-}$	$HP_2O_6^-$, $H_4P_3O_{10}^-$, $[ATP\text{-}2H]^-$, $[ATP\text{-}2H\text{-}A]^-$, PO_3^-, $[ADP\text{-}H]^- \approx H_3P_2O_7^- \approx [cAMP\text{-}H]^-$	PO_3^-, $HP_2O_6^-$, $[A\text{-}H]^-$, $[cAMP\text{-}H]^-$, $[ADP\text{-}H]^-$

[a] Photofragments and HCD fragments are listed in order of decreasing intensity.

SCHEMES AND FIGURES

Scheme 1 Chemical structures of the neutral forms of AMP, ADP and ATP.

Figure 1 a) Photodepletion (absorption) spectra of a) $[AMP-H]^-$, b) $[ADP-H]^-$, c) $[ATP-H]^-$, d) $[ADP-2H]^{2-}$, and e) $[ATP-2H]^{2-}$ across the range 4.07 – 5.77 eV. The solid lines are five-point adjacent averages of the data points.

Figure 2 Laser power measurements for photodepletion of the a) $[AMP-H]^-$, b) $[ADP-H]^-$, c) $[ATP-H]^-$, d) $[ADP-2H]^{2-}$, and e) $[ATP-2H]^{2-}$ anions, recorded at 4.9 eV.

Figure 3 Aqueous absorption spectra of ATP ($3x10^{-5}$ mol dm^{-3}) recorded at pH = 1, 2, 7 and 12.

Figure 4 Fragment production curves for a) $[AMP-H]^-$, b) $[ADP-H]^-$, c) $[ATP-H]^-$, d) $[ADP-2H]^{2-}$ and e) $[ATP-2H]^{2-}$ upon HCD between 0 and 45 % energy.

Figure 5 Photofragment mass spectra of a) $[AMP-H]^-$, b) $[ADP-H]^-$, c) $[ATP-H]^-$, d) $[ADP-2H]^{2-}$, and e) $[ATP-2H]^{2-}$ excited at 4.9 eV. * indicates the depleted parent ion signal.

Figure 6 Photofragment action spectra of the major photofragments produced following photoexcitation of mass-selected a) $[AMP-H]^-$, b) $[ADP-H]^-$, c) $[ATP-H]^-$, d) $[ADP-2H]^{2-}$, and e) $[ATP-2H]^{2-}$, across the range 4.07 – 5.77 eV. The solid lines are five-point adjacent averages of the data points.

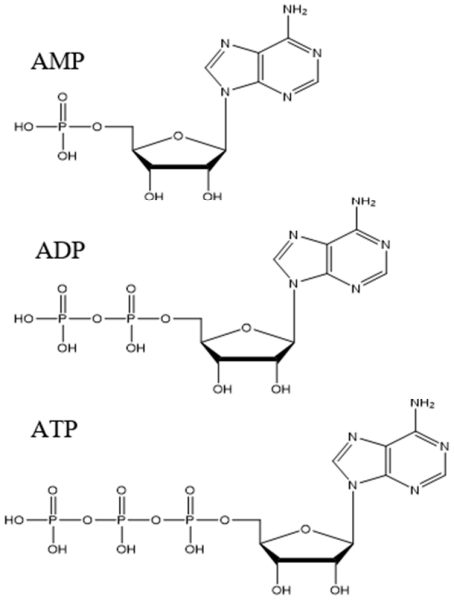

Scheme 1

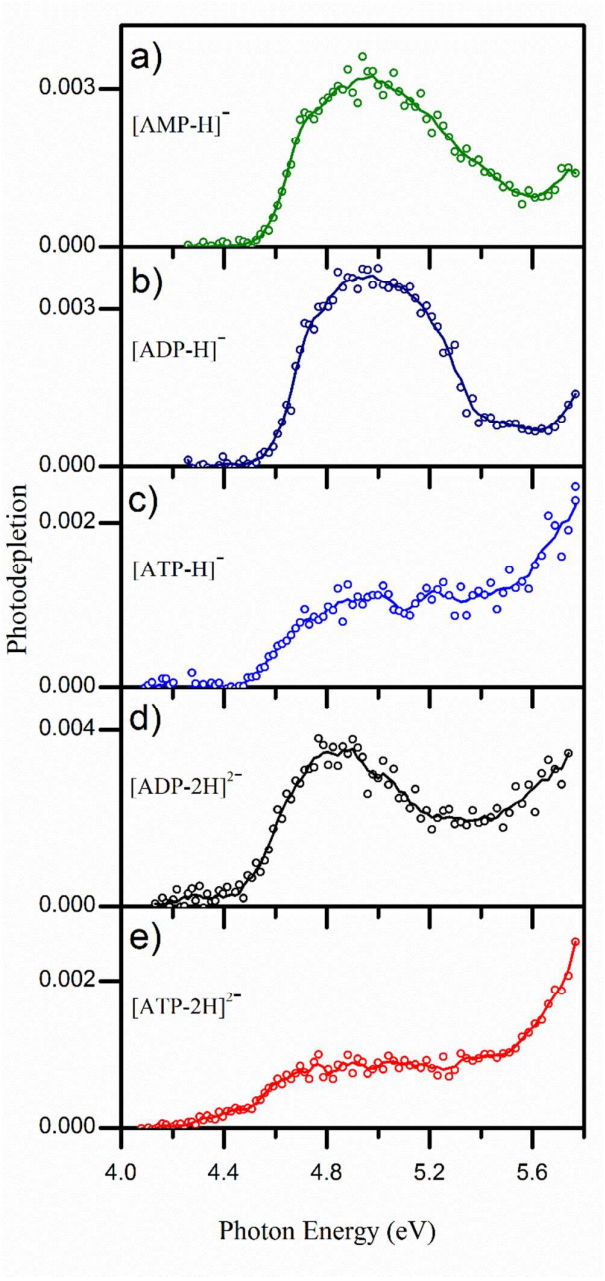
a)
[AMP-H]⁻
0.003
0.000
b)
[ADP-H]⁻
0.003
0.000
c)
[ATP-H]⁻
0.002
0.000
d)
[ADP-2H]²⁻
0.004
0.000
e)
[ATP-2H]²⁻
0.002
0.000
Photodepletion
4.0
4.4
4.8
5.2
5.6
Photon Energy (eV)

Figure 1

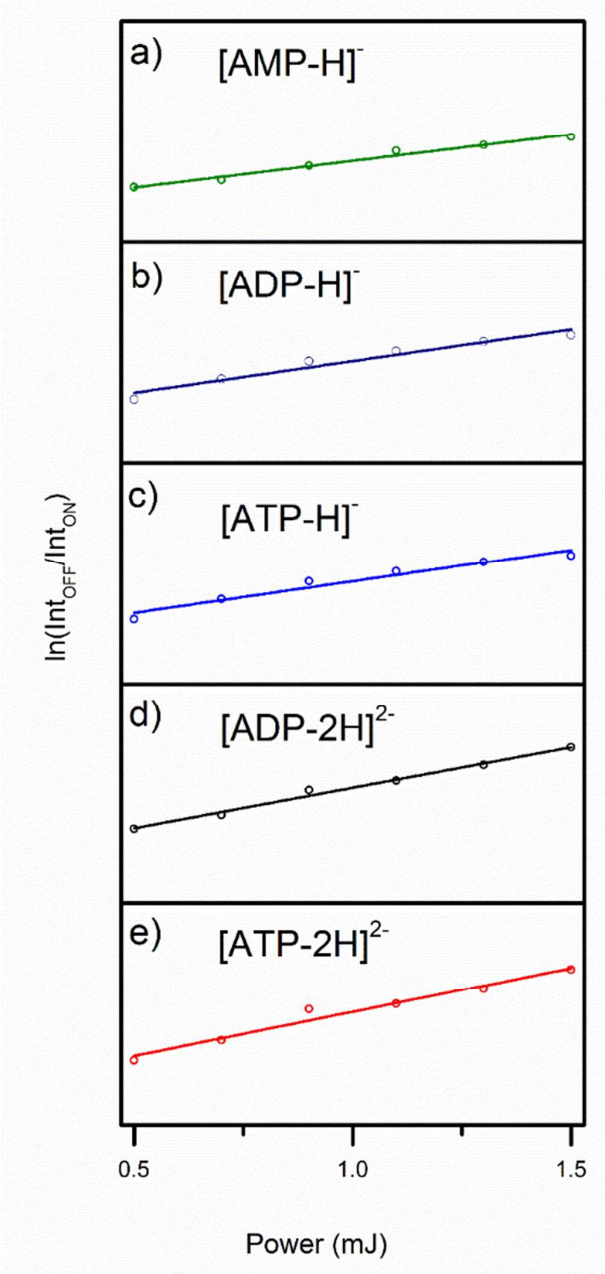
a)
[AMP-H]-
b)
[ADP-H]-
c)
[ATP-H]-
d)
[ADP-2H]2-
e)
[ATP-2H]2-
ln(IntOFF/IntON)
0.5
1.0
1.5
Power (mJ)

Figure 2

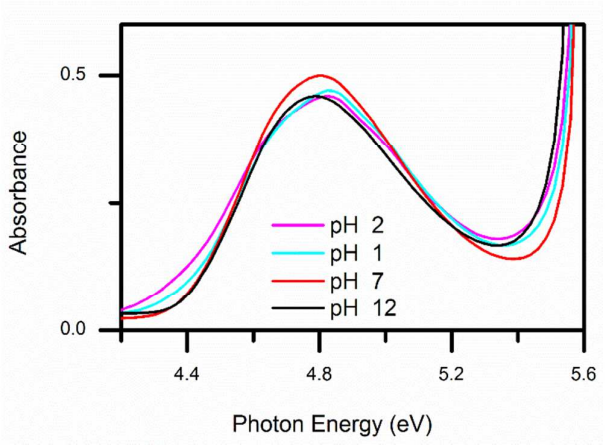

Figure 3

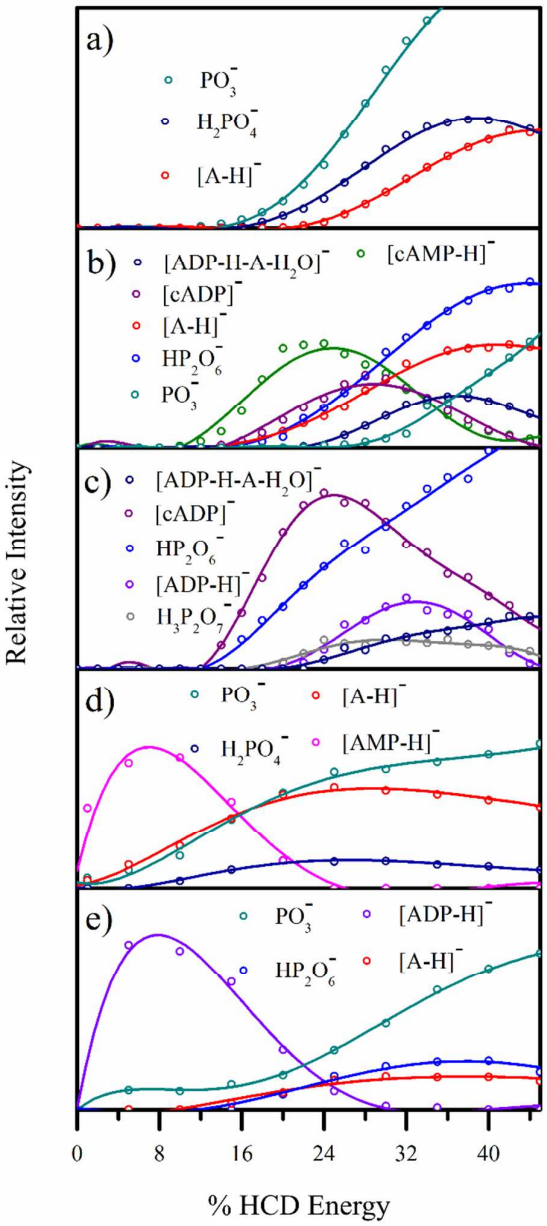
a)
PO3-
H2PO4-
[A-H]-
b)
[ADP-H-A-H2O]-
[cADP]-
[A-H]-
HP2O6-
PO3-
[cAMP-H]-
c)
[ADP-H-A-H2O]-
[cADP]-
HP2O6-
[ADP-H]-
H3P2O7-
d)
PO3-
H2PO4-
[A-H]-
[AMP-H]-
e)
PO3-
HP2O6-
[ADP-H]-
[A-H]-
Relative Intensity
0
8
16
24
32
40
% HCD Energy

Figure 4

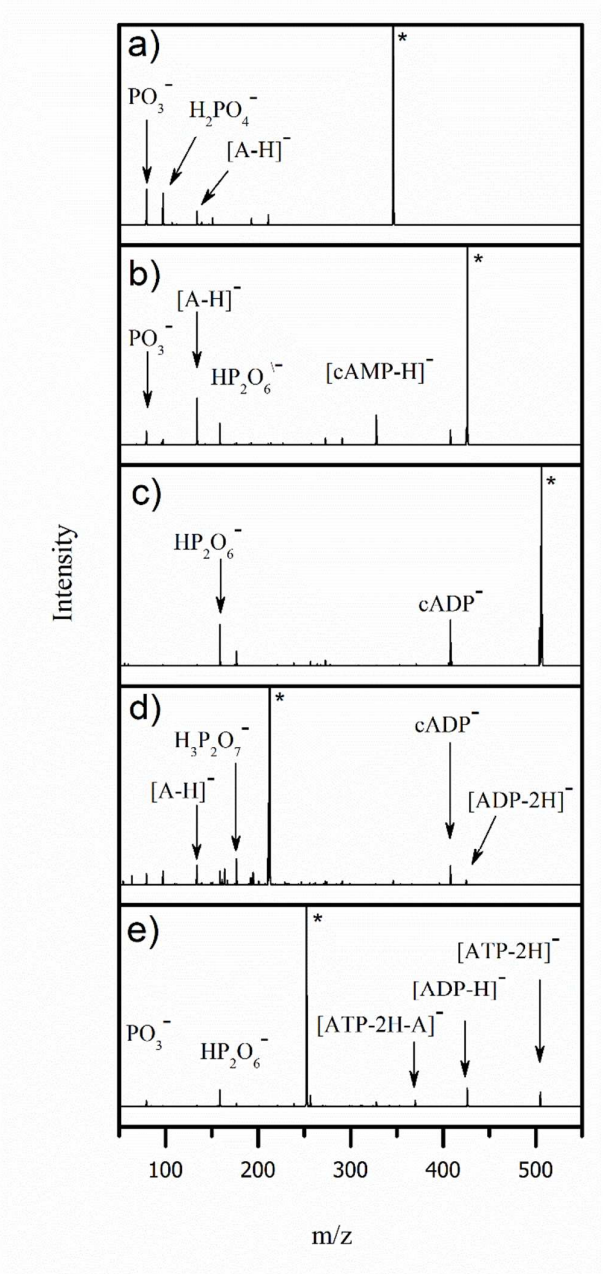
a)
PO3-
H2PO4-
[A-H]-
*
b)
[A-H]-
PO3-
HP2O6 3-
[cAMP-H]-
*
c)
HP2O6-
cADP-
*
d)
H3P2O7-
[A-H]-
cADP-
[ADP-2H]-
*
e)
[ATP-2H]-
[ADP-H]-
[ATP-2H-A]-
PO3-
HP2O6-
*
Intensity
100
200
300
400
500
m/z

Figure 5

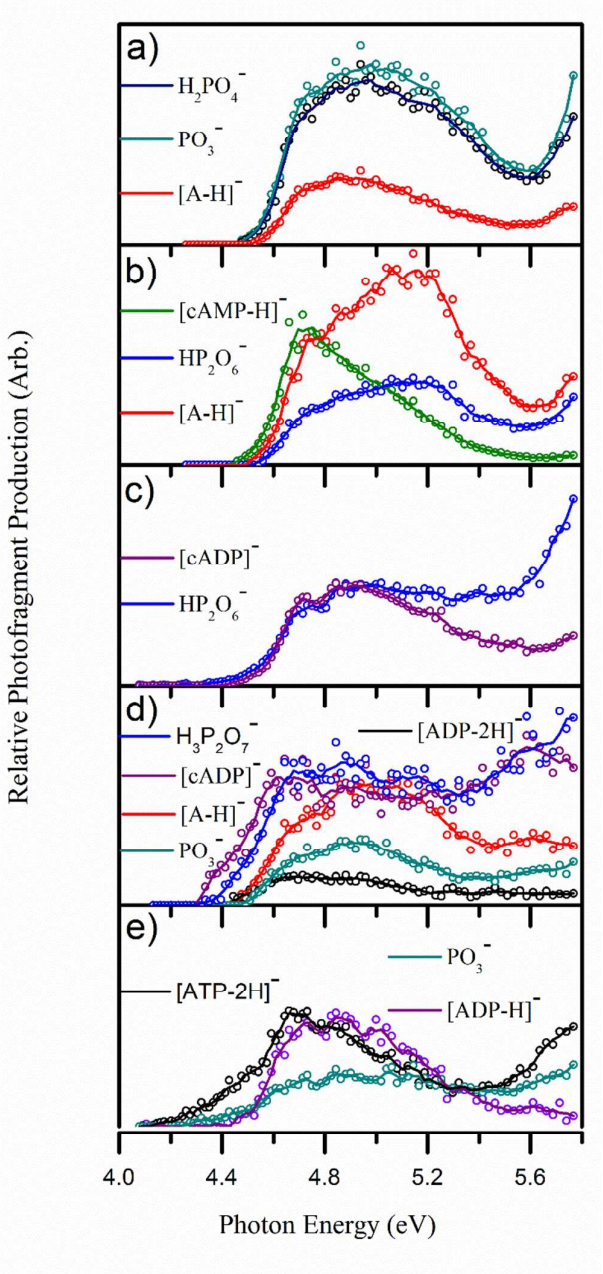
a)
$H_2PO_4^-$
PO_3^-
[A-H]$^-$
b)
[cAMP-H]$^-$
$HP_2O_6^-$
[A-H]$^-$
c)
[cADP]$^-$
$HP_2O_6^-$
d)
$H_3P_2O_7^-$
[cADP]$^-$
[A-H]$^-$
PO_3^-
[ADP-2H]$^-$
e)
[ATP-2H]$^-$
PO_3^-
[ADP-H]$^-$
Relative Photofragment Production (Arb.)
4.0
4.4
4.8
5.2
5.6
Photon Energy (eV)

Figure 6

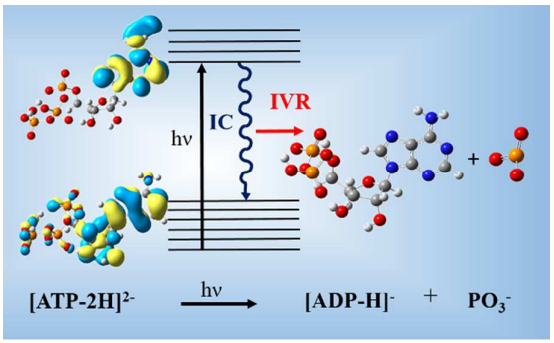

TOC Graphic

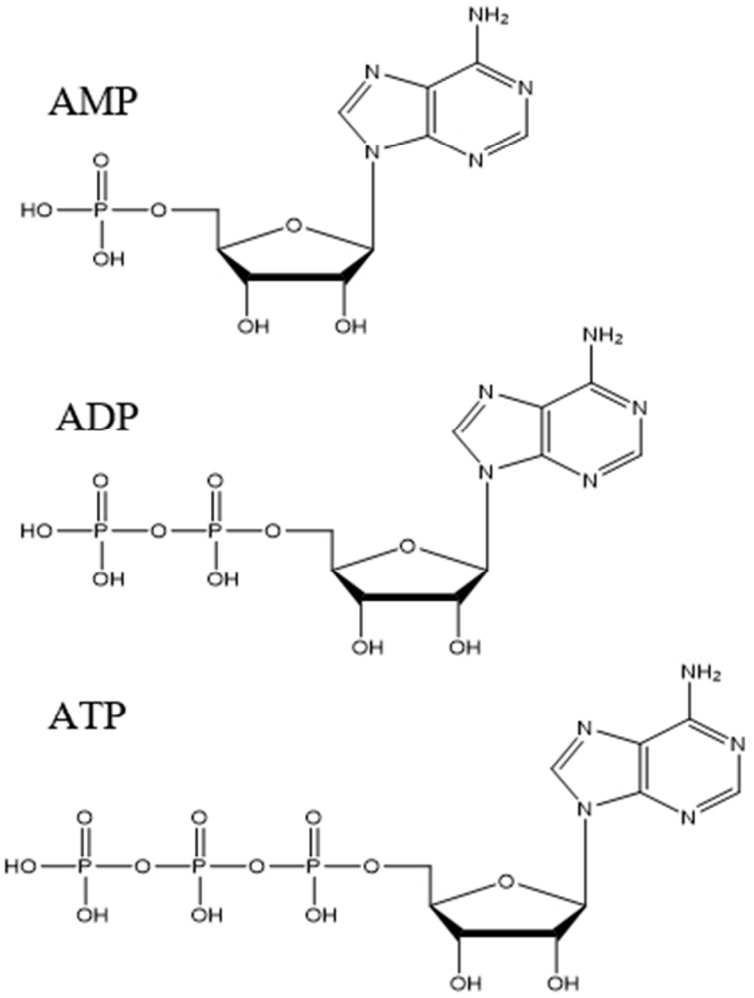

99x131mm (96 x 96 DPI)

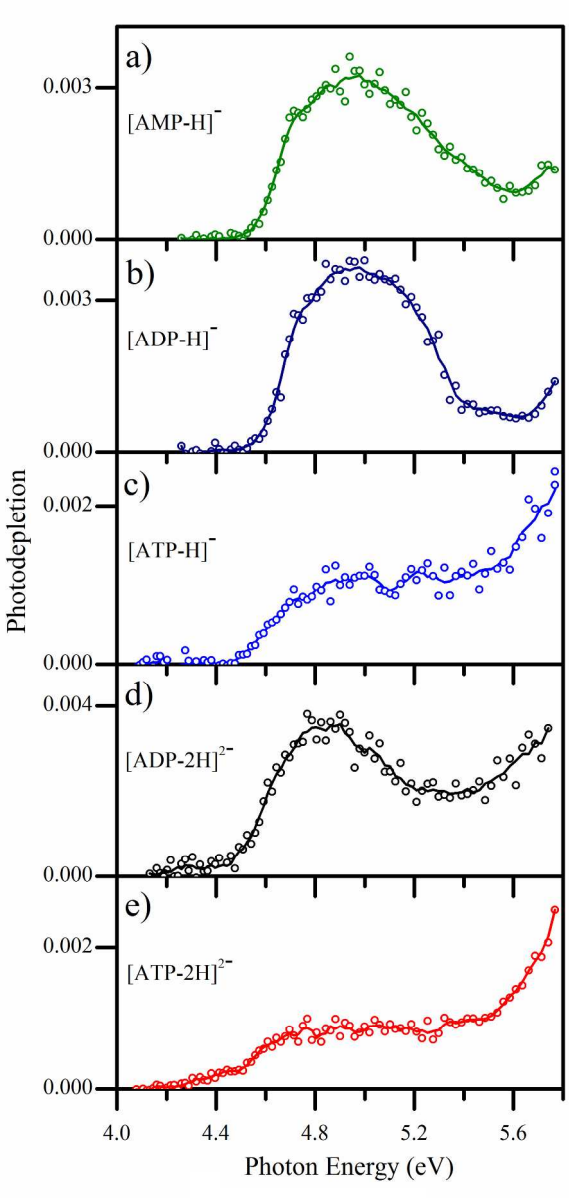

175x360mm (300 x 300 DPI)

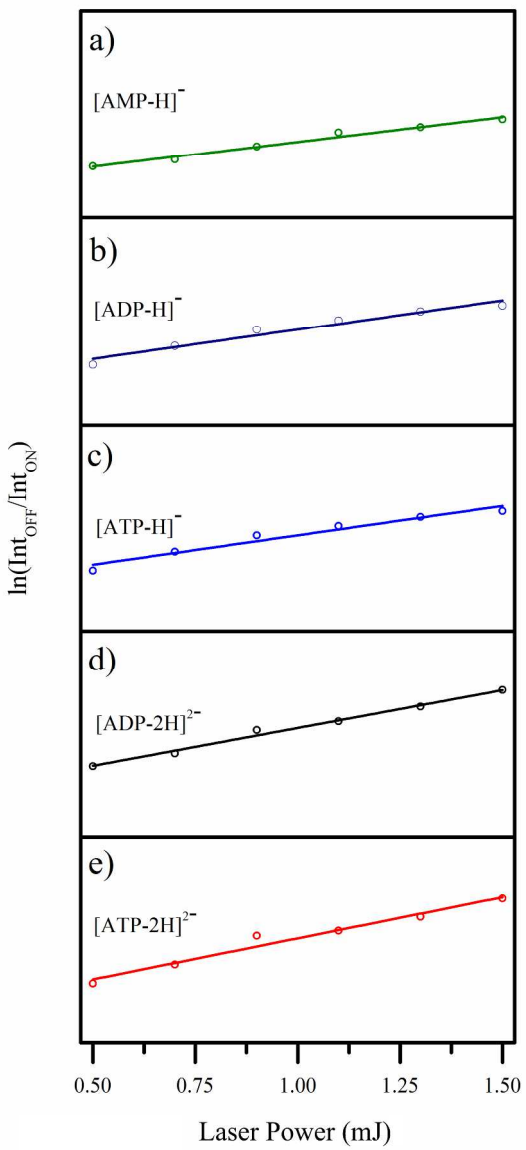

180x381mm (300 x 300 DPI)

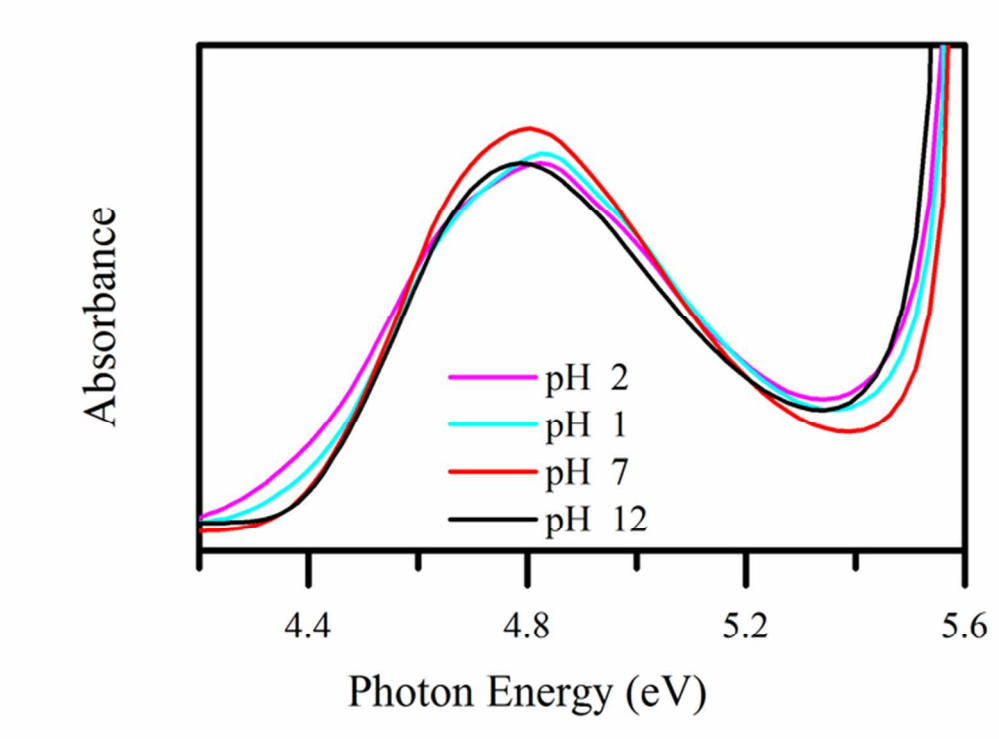

62x46mm (300 x 300 DPI)

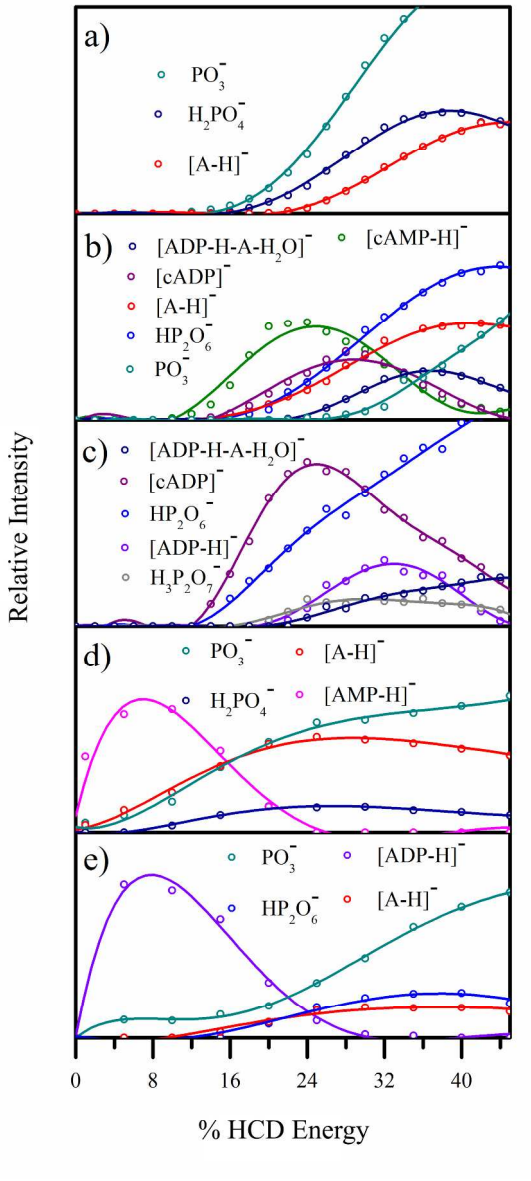

180x381mm (300 x 300 DPI)

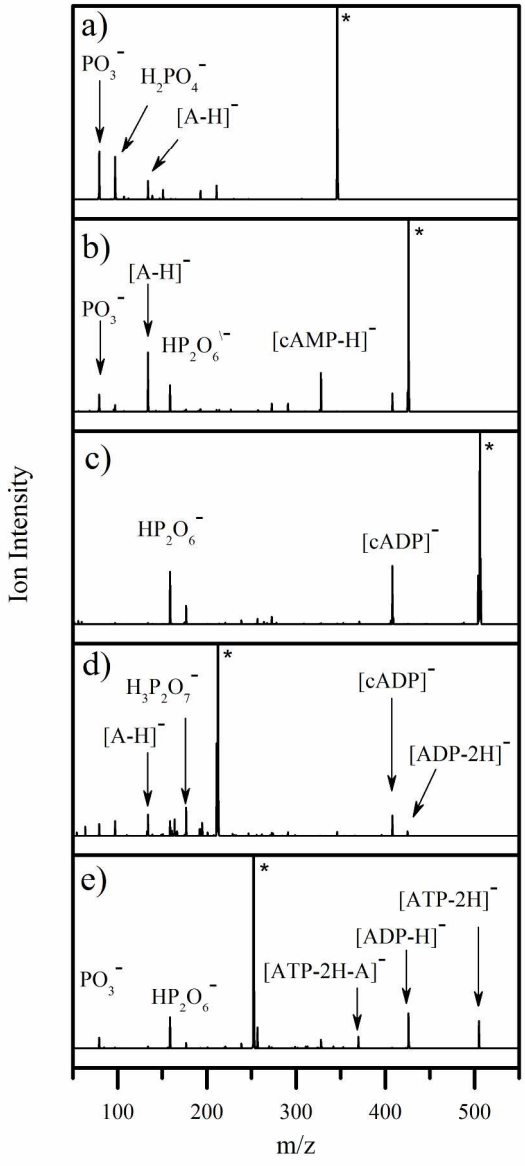

175x360mm (300 x 300 DPI)

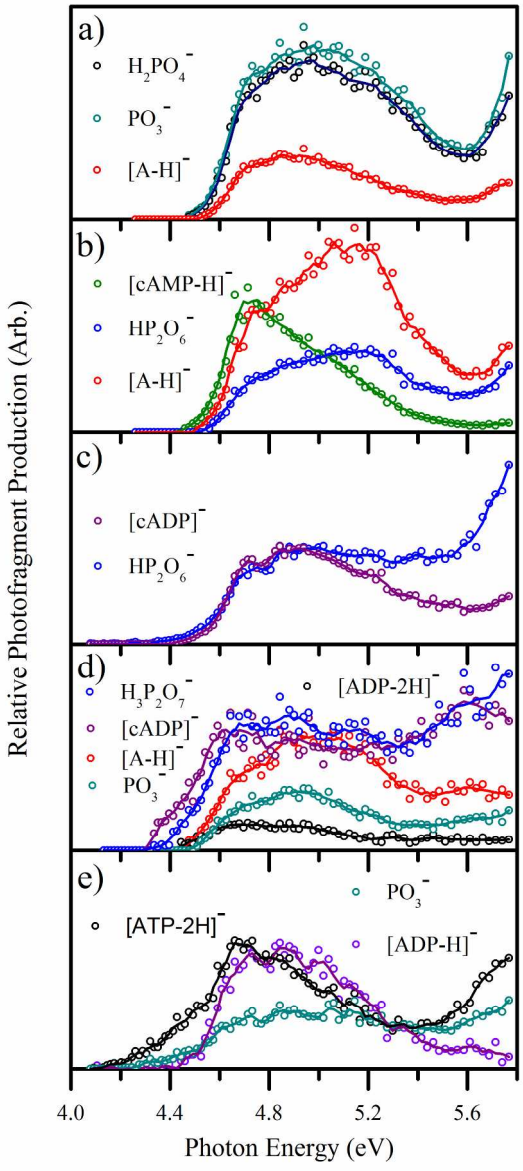

175x360mm (300 x 300 DPI)

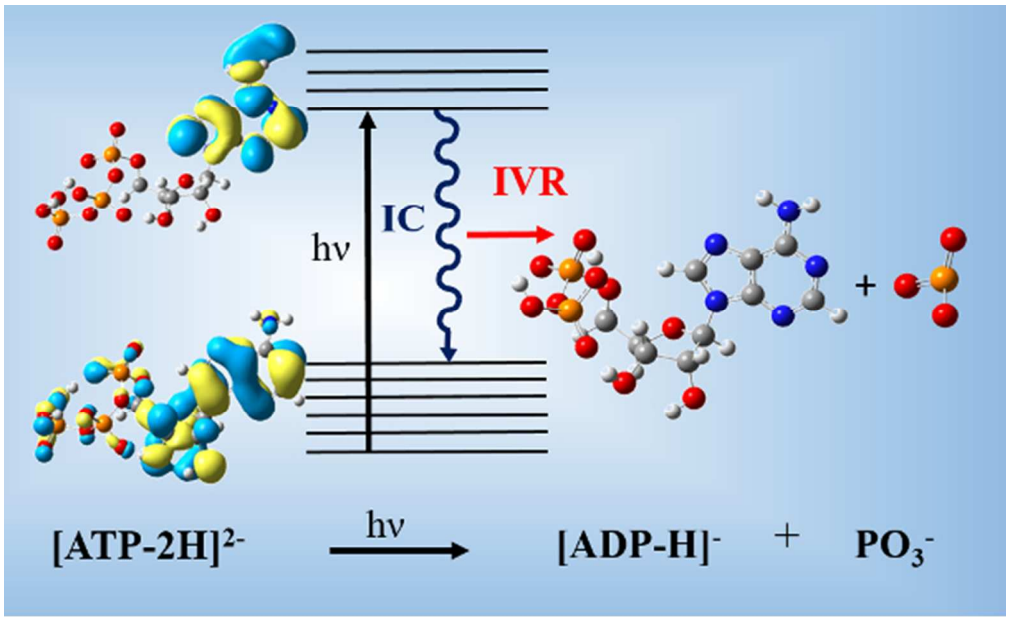

76x46mm (200 x 200 DPI)